



# Synthesis and characterization of ternary layered Nb<sub>2</sub>SB ceramics fabricated by spark plasma sintering

Yanru Qin<sup>a,1</sup>, Yanchun Zhou<sup>b,1</sup>, Longfeng Fan<sup>a</sup>, Qingguo Feng<sup>a</sup>, Salvatore Grasso<sup>a</sup>, Chunfeng Hu<sup>a,\*</sup>

<sup>a</sup> Key Laboratory of Advanced Technologies of Materials, Ministry of Education, School of Materials Science and Engineering, Southwest Jiaotong University, Chengdu 610031, China

<sup>b</sup> Science and Technology on Advanced Functional Composite Laboratory, Aerospace Research Institute of Materials & Processing Technology, Beijing 100076, China



## ARTICLE INFO

### Article history:

Received 24 March 2021

Received in revised form 5 May 2021

Accepted 7 May 2021

Available online 13 May 2021

### Keywords:

Nb<sub>2</sub>SB

Spark plasma sintering

Reaction path

Microstructure

Physical properties

Mechanical properties

## ABSTRACT

In this paper, B-containing MAX phase of Nb<sub>2</sub>SB ceramics with high purity of 96 wt% (4 wt% NbB impurity) was successfully synthesized using the molar ratio of Nb: S: B = 2: 1.3: 1 by spark plasma sintering at 1350 °C under 30 MPa. The reaction path, microstructure, physical and mechanical properties were systematically studied. It is found that the formation of Nb<sub>2</sub>SB is from the combination of Nb, NbS<sub>2</sub>, and Nb<sub>5</sub>B<sub>6</sub>, or NbB and NbS. The full dense sample (RD 99.7%) possesses the fine grains about 6 μm in length and 3.6 μm in width. The grains of Nb<sub>2</sub>SB show a layered structure, which is same to other MAX phases. The thermal expansion coefficient is  $7.1 \times 10^{-6} \text{ K}^{-1}$  in the range of 24–1100 °C. In the temperature range of 25–800 °C, the thermal diffusivity of Nb<sub>2</sub>SB ceramic increases from 5.58 mm<sup>2</sup>/s to 7.07 mm<sup>2</sup>/s. At 25 °C, the heat capacity is 0.36 J·g<sup>-1</sup>·K<sup>-1</sup>, the thermal conductivity is 13.79 W·m<sup>-1</sup>·K<sup>-1</sup>, and the electrical conductivity is  $1.17 \times 10^6 \Omega^{-1} \cdot \text{m}^{-1}$ . Additionally, the obtained Nb<sub>2</sub>SB ceramics exhibit excellent mechanical properties of Vickers hardness of 11.89 GPa (10 N load), flexural strength of 249 MPa, fracture toughness of 4.76 MPa·m<sup>1/2</sup>, and compressive strength of 1157 MPa.

© 2021 Elsevier B.V. All rights reserved.

## 1. Introduction

In the past 20 years, M<sub>n+1</sub>AX<sub>n</sub> (MAX) phases, in which M are transition metals, A are IIIA to VIA group elements, and X is carbon or nitrogen, have attracted many attentions of materials scientists due to their unique and excellent properties [1–3]. The MAX phases crystallize in P6<sub>3</sub>/mmc space group and have the hexagonal structure (symmetry number 194), and their crystal cells have highly symmetrical characteristics [4]. In the unit cells, MAX phases exhibit layer to layer microstructure, in which strong covalently bonded M–X carbides or nitrides layers are interlaced with weakly bonded “A” atom layers (alternative layers of M<sub>6</sub>X octahedral and A atoms) [5–9]. These special structure features of MAX phases make them combine the characteristics of ceramics and metals, such as high elastic modulus, high strength at elevated temperature, excellent machinability, good thermal shock resistance, good oxidation

resistance, good irradiation resistance, and high thermal and electrical conductivities, etc. [10–15]. Especially, some MAX phases, for example, Ti<sub>3</sub>SiC<sub>2</sub>, could withstand creep, mechanical fatigue, and damage tolerance under extreme conditions [16]. Thus, MAX phases have been considered as promising candidates as electrode brush materials, chemical anticorrosive materials, protective coatings, high temperature components, and friction and wear components utilized in the high temperature fields [17,18].

Until 2019, only one kind of new MAX phase containing B element at the X site was firstly synthesized by Rackl et al. [19]. He synthesized the MAX phase boride Nb<sub>2</sub>SB powder using the microwave reactor through two steps. The first step was to fabricate Nb–S compounds in the sealed argon-filled silica tube and then the second step was to sinter the mixture of Nb–S and B powders at 1200 °C for 65 h and repeat for 5 times. The black powders with purity of 92–99 wt% could be obtained. Lately, Rackl et al. discovered two new boride MAX phases: Zr<sub>2</sub>SB and Hf<sub>2</sub>SB [20]. The synthesis time was also very long up to 22 h and only very small amount powders could be achieved. Therefore, to date, no dense bulk Nb<sub>2</sub>SB ceramics with large dimension have been prepared and the physical and mechanical properties are still unknown now.

\* Correspondence to: School of Materials Science and Engineering, Southwest Jiaotong University, Chengdu 610031, China.

E-mail address: [chfhu@live.cn](mailto:chfhu@live.cn) (C. Hu).

<sup>1</sup> The authors contributed equally to this work.

In this work, in order to clearly understand the properties of Nb<sub>2</sub>SB ceramics, spark plasma sintering (SPS) method was utilized to prepare high purity dense bulks. It has been successful to fabricate the high purity Nb<sub>2</sub>SB bulks within 2 h. Under the conditions of short sintering time and high pressure, fine grains could be obtained in the dense samples, which was beneficial for the good mechanical properties [21]. The reaction path, microstructure, physical and mechanical properties were systematically characterized and compared to other S-containing MAX phases of Ti<sub>2</sub>SC and Zr<sub>2</sub>SC [22–29].

## 2. Experimental procedure

Commercial element powders of Nb (300 mesh, 99.9%, Qinhuangdao ENO High-Tech Material Development Co., LTD., China), S (5 μm, 99.0%, Qinhuangdao ENO High-Tech Material Development Co., LTD., China), and B (5 μm, 99.0%, Qinhuangdao ENO High-Tech Material Development Co., LTD., China) were utilized as raw materials to synthesize Nb<sub>2</sub>SB ceramics through a spark plasma sintering (SPS) furnace (SPS-20 T-10, Chenhua Technology Co., Ltd., China). The powder mixtures with different molar ratio of Nb: S: B were ball milled using zirconia balls in plastic jars at a rotating speed of 50 rpm for 12 h. The reaction path was systematically investigated in order to determine the optimized molar ratio and sintering parameters. The powder mixture was put into a graphite mold and compacted with a 30 MPa uniaxial pressure in the SPS furnace. The temperature was raised to 700 °C at a rate of 50 °C/min firstly, and then the temperature was increased to the designed temperature with a heating rate of 10 °C/min and held for 10 min. After sintering, the temperature was reduced to 900 °C at a rate of 50 °C/min and then cooled down to room temperature naturally. The whole sintering process was carried out in vacuum. The carburized layer on the surface of bulk sample was removed by a diamond grinding wheel. The phase compositions of all samples were examined and analyzed by an X-ray diffractometer (D8 ADVANCE, Bruker, Germany) with Cu Kα radiation (λ = 1.54178 Å). It was confirmed that the optimized molar ratio of Nb: S: B was 2: 1.3: 1 and the optimized sintering parameters were 1350 °C, 30 MPa pressure, and 10 min holding.

The density of synthesized high purity sample was measured using the Archimedes's method in deionized water. The diffraction pattern data of Nb<sub>2</sub>SB ceramic was refined by the Rietveld method to obtain the diffraction plane (*hkl*), 2θ, and *d*. The Rietveld refinement was calculated by using the GSAS-II software (free use). The fracture and etched surface (etched by a mixed acid with volumetric fraction of HNO<sub>3</sub>: HF: H<sub>2</sub>O = 1: 1: 1) of high purity bulk Nb<sub>2</sub>SB ceramic were observed by a field emission scanning electron microscopy (FSEM) (Inspect F50, FEI, US). Based on the etched SEM images, at least thirty grains of Nb<sub>2</sub>SB were collected to calculate the mean grain size.

Thermal expansion coefficient (TEC) of Nb<sub>2</sub>SB ceramic was measured using a thermal expansion analyzer (L75HD1600C, NETZSCH, Germany) in the temperature range of 24–1100 °C in nitrogen atmosphere, and the heating rate was 20 °C/min. The size of the test sample was 5 × 5 × 5 mm<sup>3</sup>. A laser thermal conductivity meter (NETZSCH LFA467, Selb, Germany) was used to measure the thermal properties in vacuum in the temperature range of 25–1100 °C. And the dimension of the test sample was Ø12.7 × 3 mm<sup>2</sup>. The electrical conductivity of Nb<sub>2</sub>SB sample at room temperature was measured by a resistivity tester (FT-300A1, Ningbo Rooko Instrument Co., Ltd., China), and the size of the sample was 1 × 1 × 10 mm<sup>3</sup>.

Vickers hardness of Nb<sub>2</sub>SB ceramic was measured through a micro-hardness tester (HVS-1000ZA, Wanheng Corp., China) under loads of 1–3 N and a Vickers hardness tester (HVS-50, Lianer Corp., China) under loads of 10–300 N. At each load, 5 points were induced

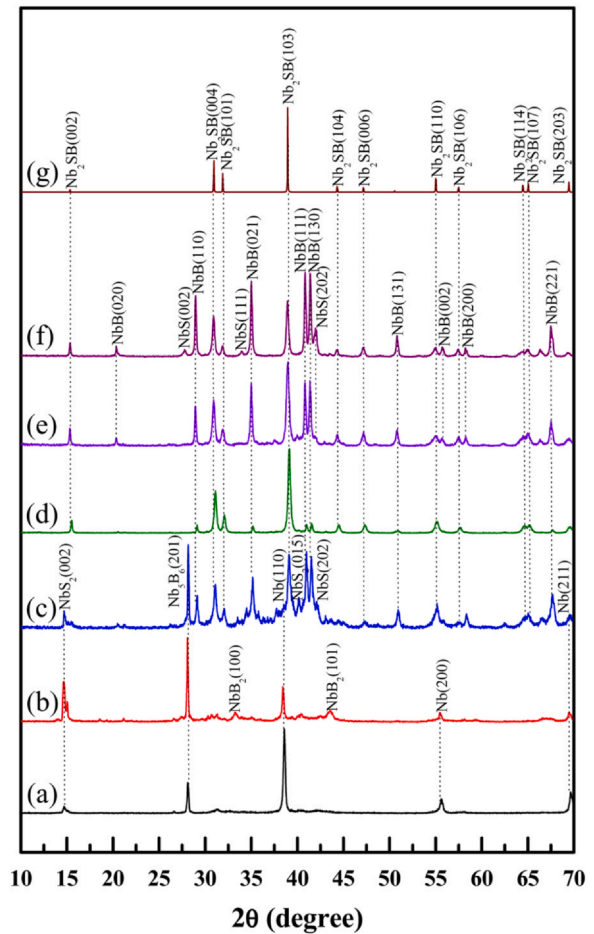


**Fig. 1.** X-ray diffraction (XRD) patterns of synthesized samples (Nb: S: B = 2: 1: 1) by spark plasma sintering at different temperature: (a) 850 °C, (b) 1050 °C, (c) 1250 °C, (d) 1350 °C, (e) 1450 °C, and (f) 1650 °C. XRD pattern of Nb<sub>2</sub>SB calculated is shown in Fig. 1(g) for comparison.

**Table 1**  
Phase compositions of samples sintered at different temperature.

Temperature (°C)	Phase composition
850	Nb, Nb <sub>2</sub> S <sub>2</sub> , Nb <sub>5</sub> B <sub>6</sub>
1050	Nb, Nb <sub>2</sub> S <sub>2</sub> , Nb <sub>5</sub> B <sub>6</sub> , NbB <sub>2</sub>
1250	Nb, Nb <sub>2</sub> S <sub>2</sub> , Nb <sub>5</sub> B <sub>6</sub> , Nb <sub>2</sub> SB, NbB, NbS
1350	Nb <sub>2</sub> SB, NbB
1450	Nb <sub>2</sub> SB, NbB, NbS
1650	Nb <sub>2</sub> SB, NbB, NbS

and measured. A universal testing machine (YC-100KN, Yice Corp., China) was used to measure flexural strength, fracture toughness, and compressive strength of Nb<sub>2</sub>SB ceramic. For each measurement, three samples were tested. The dimensions of specimens were 1.5 × 2 × 18 mm<sup>3</sup> (GB/T 6569–2006), 2 × 4 × 18 mm<sup>3</sup> (GB/T 23806–2009), and 4 × 4 × 8 mm<sup>3</sup> (GB/T 8489–2006), respectively. The flexural strength was evaluated by a three-point bending method, and the fracture toughness was measured using a single-edge notched beam (SENB) method with the notch of 2 mm in length and 0.3 mm in width. When testing the flexural strength and fracture toughness, the span was set to be 16 mm and the cross-head speeds were 0.5 and 0.05 mm/min respectively. For the compressive test, the descent speed of the cross-head was set to be 0.5 mm/min.

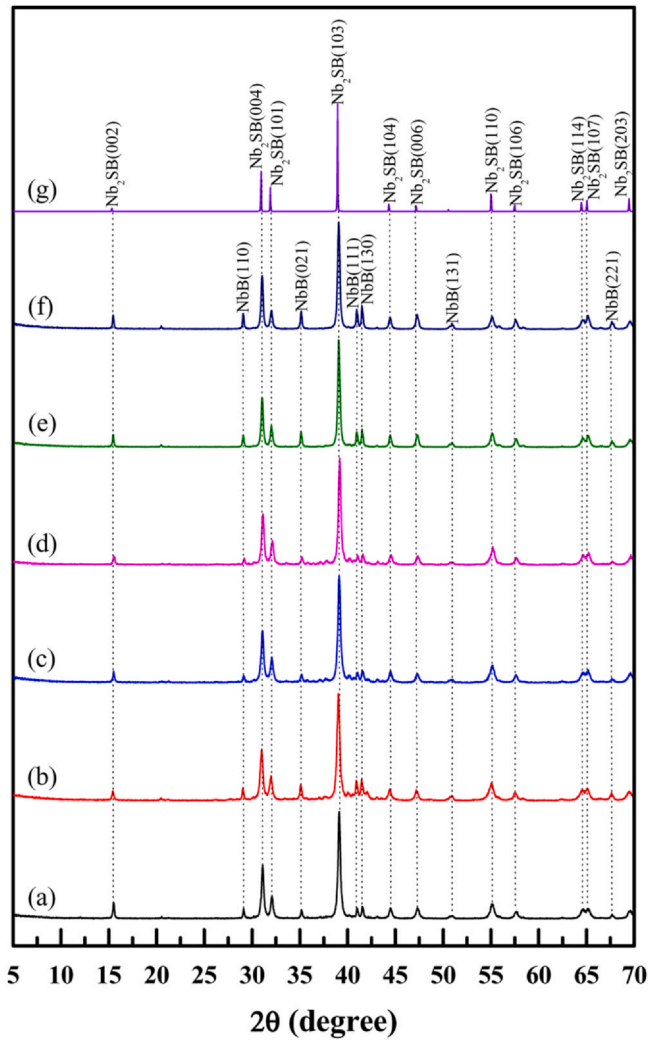


**Fig. 2.** XRD patterns of samples synthesized with different molar ratio at 1350 °C: (a) Nb: S: B = 2: 1: 1, (b) Nb: S: B = 2: 1.1: 1, (c) Nb: S: B = 2: 1.2: 1, (d) Nb: S: B = 2: 1.3: 1, (e) Nb: S: B = 2: 1.4: 1, and (f) Nb: S: B = 2: 1.5: 1. XRD pattern of Nb<sub>2</sub>SB calculated is shown in Fig. 2(g) for comparison.

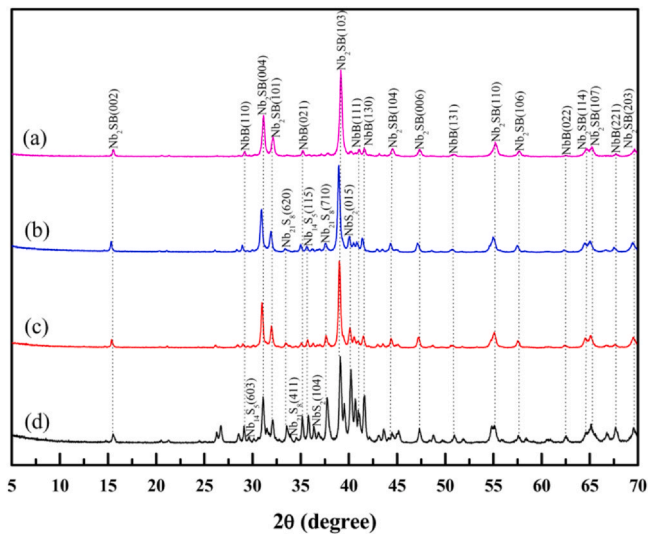


**Fig. 3.** XRD spectra of samples synthesized with different ratio at 1350 °C: (a) Nb: S: B = 2: 1.3: 1, (b) Nb: S: B = 2: 1.3: 0.9, (c) Nb: S: B = 2: 1.3: 0.8, and (d) Nb: S: B = 2: 1.3: 0.7.

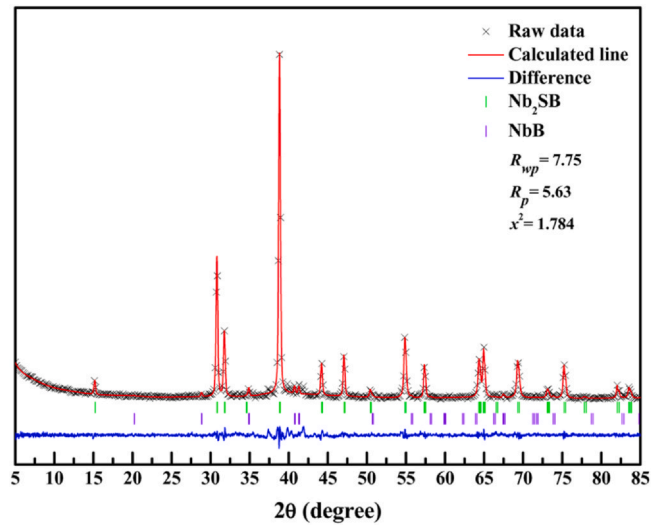


**Fig. 4.** Comparison between the observed (black cross x) and calculated XRD (red line) patterns of Nb<sub>2</sub>SB. The blue line indicates the difference between the observed and calculated XRD patterns. The green and purple vertical short lines below the patterns represent the peak positions of Nb<sub>2</sub>SB and NbB phases, respectively.

### 3. Results and discussion

#### 3.1. Synthesis of Nb<sub>2</sub>SB ceramics

Fig. 1(a)–(f) show the X-ray diffraction (XRD) patterns of the samples (Nb : S : B = 2 : 1 : 1) sintered by spark plasma sintering at 850–1650 °C. The theoretical XRD spectra of Nb<sub>2</sub>SB ceramic used for comparison is shown in Fig. 1(g). The phase compositions of samples sintered at the different temperatures are summarized in Table 1. It is seen that at 850 °C the formed phases are NbS<sub>2</sub> and Nb<sub>5</sub>B<sub>6</sub> (Fig. 1(a)), thus, the reaction equations could be described as:



Here, because B and S are relatively light elements, they could not be detected in the XRD pattern. When further increasing the temperature to be 1050 °C, more NbS<sub>2</sub> and Nb<sub>5</sub>B<sub>6</sub> appear and NbB<sub>2</sub> phase was also detected with the consumption of Nb (Fig. 1(b)). The reaction might be:



Interestingly, it is observed that at 1250 °C Nb<sub>2</sub>SB has been fabricated with the decreasing content of Nb, NbS<sub>2</sub>, and Nb<sub>5</sub>B<sub>6</sub>. Also, NbB<sub>2</sub> phase was consumed, and other phases of NbB and NbS were formed (Fig. 1(c)). The formation reactions could probably be:



When sintering the sample at 1350 °C, all of the Nb, Nb<sub>5</sub>B<sub>6</sub>, and NbS<sub>2</sub> phases disappear and only Nb<sub>2</sub>SB and NbB phases exist in the sample (Fig. 1(d)). Therefore, the formation reaction might be:



However, at the sintering temperature above 1450 °C, new impurity of NbS phase was examined and more NbB phase appears (Fig. 1(e)), which should be ascribed to the decomposition of Nb<sub>2</sub>SB. The decomposition equation is:



**Table 2**  
Calculated and observed data of reflections,  $2\theta$ ,  $d$ -spacing, and intensities of Nb<sub>2</sub>SB.

(hkl)	$2\theta_{\text{Cal.}}$ (°)	$2\theta_{\text{Obs.}}$ (°)	$d_{\text{Cal.}}$ (Å)	$d_{\text{Obs.}}$ (Å)	$I/I_{0\text{Cal.}}$ (%)	$I/I_{0\text{Obs.}}$ (%)
(0 0 2)	15.329	15.342	5.776	5.771	4.522	3.321
(1 0 0)	30.935	30.927	2.888	2.890	30.186	34.239
(0 0 4)	30.941	30.968	2.888	2.885	12.781	13.934
(1 0 1)	31.912	31.906	2.802	2.803	24.995	24.060
(1 0 2)	34.697	34.696	2.583	2.583	0.035	0.325
(1 0 3)	38.949	38.955	2.310	2.310	100	100
(1 0 4)	44.320	44.334	2.042	2.042	10.270	7.968
(0 0 6)	47.170	47.213	1.925	1.924	8.269	8.937
(1 0 5)	50.550	50.573	1.804	1.803	1.784	2.077
(1 1 0)	55.023	55.008	1.668	1.668	27.647	26.230
(1 1 2)	57.474	57.464	1.602	1.602	0.872	0.361
(1 0 6)	57.481	57.514	1.602	1.601	8.443	7.342
(2 0 0)	64.469	64.451	1.444	1.445	3.518	4.027
(1 1 4)	64.472	64.474	1.444	1.444	9.545	9.652
(0 0 8)	64.482	64.544	1.444	1.443	1.356	1.295
(2 0 1)	65.032	65.015	1.433	1.433	3.244	2.820
(1 0 7)	65.042	65.085	1.433	1.432	11.271	10.311
(2 0 2)	66.707	66.694	1.401	1.401	0.017	0.050
(2 0 3)	69.454	69.445	1.352	1.352	17.209	17.458
(2 0 4)	73.220	73.218	1.292	1.292	2.221	1.614
(1 0 8)	73.230	73.284	1.291	1.291	0.947	1.360
(1 1 6)	75.340	75.361	1.260	1.260	12.065	13.304
(2 0 5)	77.956	77.962	1.225	1.225	0.487	0.650
(1 0 9)	82.105	82.173	1.173	1.172	4.066	4.247
(2 0 6)	83.637	83.653	1.155	1.155	2.917	2.600
(0 0 10)	83.649	83.738	1.155	1.154	1.446	1.150
(2 1 0)	89.756	89.728	1.092	1.092	3.023	3.519
(1 1 8)	89.768	89.812	1.092	1.091	3.520	3.535

Even at the temperature of 1650 °C, Nb<sub>2</sub>SB phase still exists (Fig. 1(f)), indicating that it is a candidate to be used in the high temperature field.

Based on the XRD analysis, it is determined that the optimum sintering temperature of Nb<sub>2</sub>SB ceramic is 1350 °C because only NbB impurity coexists in the sample. Similar to Ti<sub>2</sub>SC [25], the formation of Nb<sub>2</sub>SB is from the combination of Nb, NbS<sub>2</sub>, and Nb<sub>5</sub>B<sub>6</sub>, or NbB and NbS.

In order to fabricate high purity Nb<sub>2</sub>SB ceramics, more sulfur was added to compensate the loss during the sintering because the melting point of sulfur is only 112 °C which leads to the evaporation at high temperature. Fig. 2(a)–(f) display the XRD spectra of Nb<sub>2</sub>SB samples sintered at 1350 °C with the different molar ratio of Nb, S, and B. It can be clearly seen that when the molar ratio of Nb: S: B is 2: 1.3: 1 the synthesized Nb<sub>2</sub>SB sample has the least impurity of NbB, corresponding to the weakest diffraction peak intensities of (110), (111), and (130) planes (Fig. 2(d)). Therefore, the optimized molar ratio to obtain high purity Nb<sub>2</sub>SB is Nb: S: B = 2: 1.3: 1.

Furthermore, in order to remove the impurity of NbB, the B content in the initial mixture powders was also changed. Fig. 3(a)–

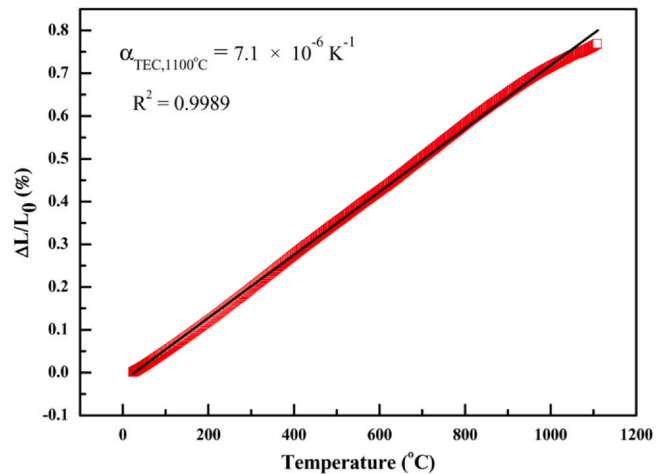


**Fig. 6.** The temperature dependence of thermal expansion measured in nitrogen from 24 °C to 1100 °C.

(d) show the XRD patterns of sintered Nb<sub>2</sub>SB samples prepared by using the different B additive. It is found that with the decreasing B content the impurities of Nb-S compounds such as Nb<sub>21</sub>S<sub>8</sub>, Nb<sub>14</sub>S<sub>5</sub>, and NbS<sub>2</sub> appear more. So, it is not a wise way to reduce boron content. Finally, the optimized synthesis parameters of high purity Nb<sub>2</sub>SB ceramics sintered by spark plasma sintering are determined as Nb: S: B = 2: 1.3: 1, 1350 °C, 10 min holding, and 30 MPa pressure.

Since the discovery of Nb<sub>2</sub>SB phase, no full set of XRD data was given in the published paper [19]. Here, it is necessary to clearly describe the diffraction data to make this compound understood more. Fig. 4 shows the XRD pattern and Rietveld refinement result of high purity Nb<sub>2</sub>SB ceramic. The Rietveld refined accuracies are  $R_{\text{wp}} = 7.75$  and  $R_p = 5.63$ , high enough to supply the credible data. Additionally, it was calculated that the sample contained 96 wt% Nb<sub>2</sub>SB and 4 wt% NbB, suitable to be characterized for physical and mechanical properties. The refined crystal parameters are  $a = 3.336$  Å and  $c = 11.541$  Å, which are close to the reported values ( $a = 3.335$  Å and  $c = 11.551$  Å) [19]. Table 2 summarizes the calculated and observed data of diffraction plane,  $2\theta$ , interlayer spacing  $d$ , and peak intensity of Nb<sub>2</sub>SB.

### 3.2. Microstructure characterization

The density of bulk Nb<sub>2</sub>SB sample was measured using the Archimedes' principle, which is 6.84 g/cm<sup>3</sup>, corresponding to the high relative density of 99.7%. The scanning electron microscope (SEM) image of the polished surface after etching is shown in

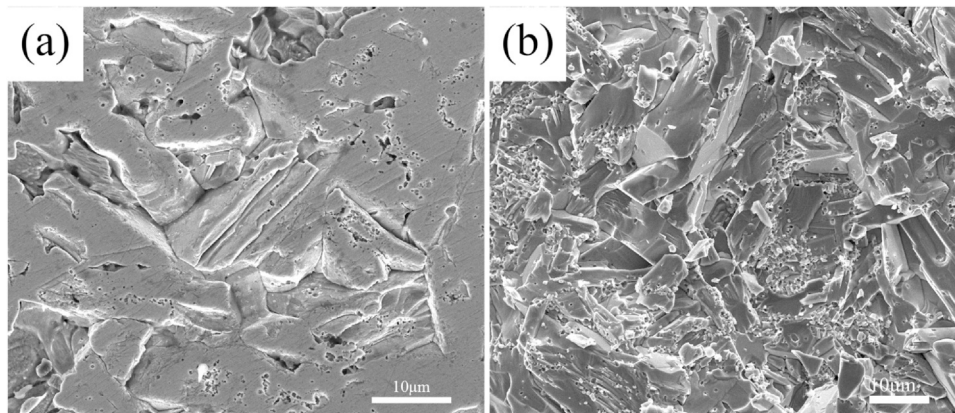


**Fig. 5.** Scanning electron microscope (SEM) micrographs of (a) etched and (b) fracture surface of Nb<sub>2</sub>SB ceramic.

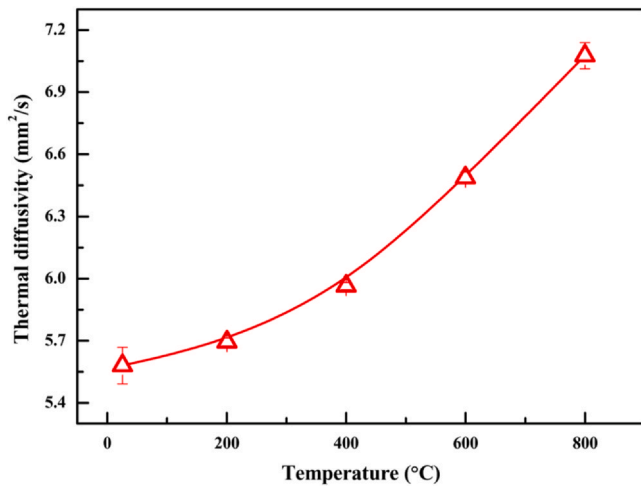


Fig. 7. Thermal diffusivity of Nb<sub>2</sub>SB ceramic measured in vacuum from room temperature to 800 °C.

Fig. 5(a). It is seen that the grains of Nb<sub>2</sub>SB grow randomly in all directions, and no texture microstructure could be observed. The laminar microstructure of individual grain exhibits the typical layer character, similar to those of other MAX phases of Ti<sub>2</sub>SC and Zr<sub>2</sub>SC. The calculated mean grain size is about 6 μm in length and 3.6 μm in width, showing the fine microstructure. Additionally, by observing the fracture surface of Nb<sub>2</sub>SB ceramic, it is found that transgranular fracture is the main damage mode and nearly no layered character of grains could be observed (Fig. 5(b)), which means that the as-prepared Nb<sub>2</sub>SB ceramic would probably exhibit the high brittleness.

### 3.3. Physical properties evaluation

Fig. 6 displays the thermal expansion curve of Nb<sub>2</sub>SB ceramic measured from 24 to 1100 °C. After linear fitting, an equation versus temperature was obtained and drawn as a straight line. The equation of  $\alpha_{TEC,1100}^{\circ C} = -0.01984 + 0.000739 T$  with a R-square of 0.9989 could be achieved. The mean thermal expansion coefficient in the range of

24–1100 °C was calculated as  $7.1 \times 10^{-6} K^{-1}$ , which is lower than those of Ti<sub>2</sub>SC ( $8.4\text{--}9.3 \times 10^{-6} K^{-1}$ ) [30] and Zr<sub>2</sub>SC ( $8.8 \times 10^{-6} K^{-1}$ ) [27].

Fig. 7 shows the temperature dependence of thermal diffusivity. The result exhibits that the thermal diffusivity of Nb<sub>2</sub>SB ceramic increases from 5.58 mm<sup>2</sup>/s to 7.07 mm<sup>2</sup>/s in the temperature range of 25–800 °C. It seems that although the thermal diffusivity of Nb<sub>2</sub>SB increases with the increment of temperature, the thermal diffusivity is still a low value.

The heat capacity and thermal conductivity of Nb<sub>2</sub>SB ceramic are shown in Fig. 8. As the temperature rises from room temperature to 800 °C, the heat capacity shows an upgraded tendency from 0.36 J·g<sup>-1</sup>·K<sup>-1</sup> to 0.49 J·g<sup>-1</sup>·K<sup>-1</sup>, which fits a third-order polynomial [31]. At the same temperature range, the thermal conductivity increases from 13.79 W·m<sup>-1</sup>·K<sup>-1</sup> to 23.59 W·m<sup>-1</sup>·K<sup>-1</sup>. The heat capacity and thermal conductivity of Nb<sub>2</sub>SB ceramic at room temperature are lower than those of Ti<sub>2</sub>SC (0.57–0.59 J·g<sup>-1</sup>·K<sup>-1</sup>, 53.4–60 W·m<sup>-1</sup>·K<sup>-1</sup>) [22,25,30], and also lower than those of Zr<sub>2</sub>SC (0.4 J·g<sup>-1</sup>·K<sup>-1</sup>, 38 W·m<sup>-1</sup>·K<sup>-1</sup>) [27] at 100 °C.

In addition, the electrical conductivity of Nb<sub>2</sub>SB ceramic was measured as  $1.17 \times 10^6 \Omega^{-1}\cdot m^{-1}$  at room temperature. In comparison with that of Ti<sub>2</sub>SC ( $1.85\text{--}1.92 \times 10^6 \Omega^{-1}\cdot m^{-1}$ ), the conductivity value of Nb<sub>2</sub>SB is smaller.

### 3.4. Mechanical properties evaluation

The physical and mechanical properties of Nb<sub>2</sub>SB ceramic are listed in Table 3 and compared to other typical S-containing MAX phases of Ti<sub>2</sub>SC and Zr<sub>2</sub>SC. It is seen that the flexural strength of Nb<sub>2</sub>SB ceramic is  $249 \pm 17$  MPa, lower than both of Ti<sub>2</sub>SC (394 MPa) [25] and Zr<sub>2</sub>SC ( $275 \pm 10$  MPa) [27]. The fracture toughness of Nb<sub>2</sub>SB is  $4.76 \pm 0.36$  MPa·m<sup>1/2</sup>, which is close to that of Ti<sub>2</sub>SC (4–6 MPa·m<sup>1/2</sup>) [22,25,30]. The measured compressive strength of Nb<sub>2</sub>SB is  $1157 \pm 73$  MPa, which is greatly higher than that of Ti<sub>2</sub>SC (736 MPa) [25].

The hardness and damage tolerance of Nb<sub>2</sub>SB ceramic were evaluated by measuring Vickers hardness as a function of indentation load, as shown in Fig. 9. At a low indent load of 1 N, the Vickers hardness of Nb<sub>2</sub>SB has a high value of 13.34 GPa. With the increasing load, the hardness value decreases correspondingly to approach a

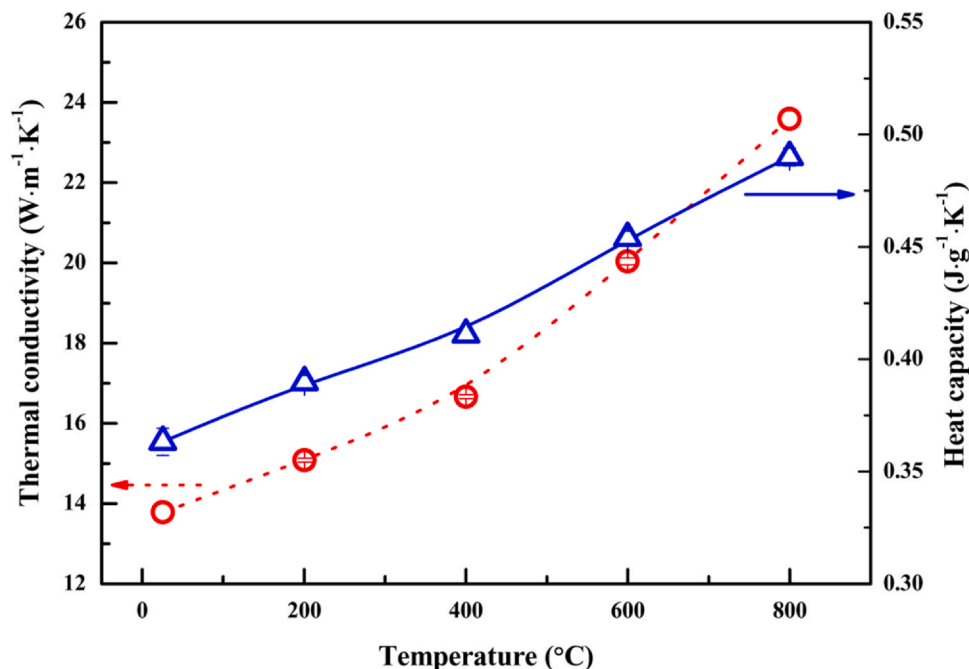
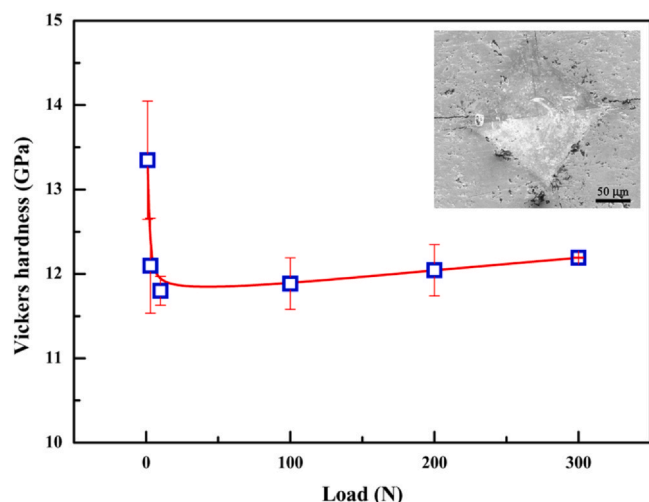


Fig. 8. Temperature dependence of thermal conductivity and thermal capacity of Nb<sub>2</sub>SB ceramic measured in the temperature range of 25–800 °C.

**Table 3**  
Comparative analysis of physical and mechanical properties of Nb<sub>2</sub>SB, Ti<sub>2</sub>SC, and Zr<sub>2</sub>SC.

Properties	Nb <sub>2</sub> SB	Ti <sub>2</sub> SC [22,25,30]	Zr <sub>2</sub> SC [27]
Molecular weight (g/mol)	228.67	139.8	226.5
Density (g/cm <sup>3</sup> )	6.84	4.60–4.62	–
Vickers hardness (GPa) (10 N)	11.8 ± 0.37	6.7–8	6.4
Flexural strength (MPa)	249 ± 17	394	275 ± 10
Fracture toughness (MPa·m <sup>1/2</sup> )	4.76 ± 0.36	4–6	–
Compressive strength (MPa)	1157 ± 73	736	–
Electrical conductivity (×10 <sup>6</sup> Ω <sup>-1</sup> ·m <sup>-1</sup> ) (25 °C)	1.17	1.85–1.92	–
Thermal expansion coefficient (×10 <sup>-6</sup> K <sup>-1</sup> )	7.1	8.4–9.3	8.8
Heat capacity, C <sub>p</sub> (J·g <sup>-1</sup> ·K <sup>-1</sup> ) (25 °C)	0.36	0.57–0.59	0.5 (100 °C)
Thermal conductivity (W·m <sup>-1</sup> ·K <sup>-1</sup> ) (25 °C)	13.79	53.4–60	38 (100 °C)



**Fig. 9.** Vickers hardness as a function of indentation load. Inset image is an indent induced at 300 N.

constant, presenting the typical rule of *Indentation-Size Effect (ISE)* [32–36]. At the load of 10 N, the Vickers hardness of Nb<sub>2</sub>SB is 11.89 ± 0.37 GPa, higher than those of Ti<sub>2</sub>SC (6.7–8 GPa) [22,25,30] and Zr<sub>2</sub>SC (6.4 GPa) [27]. In addition, the indent induced at 300 N is shown in the inset image, which has a square shape. No grains pushing-out, grains crushing, and delamination can be observed and at the diagonals the cracks appear. It is concluded that Nb<sub>2</sub>SB ceramic has the strong bonding in the crystal structure, resulting in the high hardness.

#### 4. Conclusions

High purity B-containing MAX phase of Nb<sub>2</sub>SB ceramic has been successfully fabricated by spark plasma sintering. The reaction path, microstructure, physical and mechanical properties were systematically investigated. The obtained conclusions are listed as follows:

- (1) The optimized molar ration to synthesize high purity Nb<sub>2</sub>SB ceramic is Nb: S: B = 2: 1.3: 1, and the optimum sintering parameters are 1350 °C, 10 min holding, and 30 MPa pressure. The formation of Nb<sub>2</sub>SB is from the combination of Nb, NbS<sub>2</sub>, and Nb<sub>5</sub>B<sub>6</sub>, or NbB and NbS. The obtained dense Nb<sub>2</sub>SB ceramic has the high purity of 96 wt% and high relative density of 99.7%. The mean grain size is about 6 μm in length and 3.6 μm in width.
- (2) The measured thermal expansion coefficient of Nb<sub>2</sub>SB ceramic in the range of 24–1100 °C is 7.1 × 10<sup>-6</sup> K<sup>-1</sup>. The thermal diffusivity of Nb<sub>2</sub>SB ceramic increases from 5.58 mm<sup>2</sup>/s at 25 °C to 7.07 mm<sup>2</sup>/s at 800 °C with the increment of temperature. The heat capacity and thermal conductivity at 25 °C are 0.36 J·g<sup>-1</sup>·K<sup>-1</sup>

and 13.79 W·m<sup>-1</sup>·K<sup>-1</sup>, respectively. And the electrical conductivity at room temperature is 1.17 × 10<sup>6</sup> Ω<sup>-1</sup>·m<sup>-1</sup>.

- (3) The measured flexural strength and fracture toughness of Nb<sub>2</sub>SB ceramic are 249 MPa and 4.76 MPa·m<sup>1/2</sup>, respectively. The compressive strength of Nb<sub>2</sub>SB is 1157 MPa and the Vickers hardness is 11.89 GPa. The excellent physical and mechanical properties endow Nb<sub>2</sub>SB ceramic as the good candidate utilized in the high temperature fields as structural-functional integrated materials.

#### CRediT authorship contribution statement

**Yanru Qin:** Writing - original draft. **Yanchun Zhou:** Investigation. **Longfeng Fan:** Writing - review & editing. **Qingguo Feng:** Writing - review & editing. **Salvatore Grasso:** Writing - review & editing. **Chunfeng Hu:** Supervision, Project administration, Funding acquisition.

#### Declaration of Competing Interest

The authors declare that they have no known competing financial interests or personal relationships that could have appeared to influence the work reported in this paper.

#### Acknowledgments

This work is supported by the Natural Sciences Foundation of China (No. 52072311), Outstanding Young Scientific and Technical Talents in Sichuan Province (2019JDJQ0009), the Opening Project of State Key Laboratory of Green Building Materials, and the Open Project of State Key Laboratory Cultivation Base for Nonmetal Composites and Functional Materials (20kfhg17).

#### References

- [1] P.A. Miloserdov, V.A. Gorshkov, I.D. Kovalev, D.Y. Kovalev, High-temperature synthesis of cast materials based on Nb<sub>2</sub>AlC MAX phase, *Ceram. Int.* 45 (2019) 2689–2691, <https://doi.org/10.1016/j.ceramint.2018.10.198>
- [2] V.A. Gorshkov, A.V. Karpov, D.Y. Kovalev, A.E. Sychev, Synthesis, structure and properties of material based on V<sub>2</sub>AlC MAX phase, *Phys. Met. Metallogr.* 121 (2020) 765–771, <https://doi.org/10.1134/S0031918x20080037>
- [3] P. Yao, Y. Qian, W. Li, C. Li, J. Zuo, J. Xu, M. Li, Exploration of dielectric and microwave absorption properties of quaternary MAX phase ceramic (Cr<sub>2/3</sub>Ti<sub>1/3</sub>)<sub>3</sub>AlC<sub>2</sub>, *Ceram. Int.* 46 (2020) 22919–22926, <https://doi.org/10.1016/j.ceramint.2020.06.065>
- [4] S.R.G. Christopoulos, N. Kelaidis, A. Chroneos, Defect processes of M<sub>3</sub>AlC<sub>2</sub> (M = V, Zr, Ta, Ti) MAX phases, *Solid State Commun.* 261 (2017) 54–56, <https://doi.org/10.1016/j.ssc.2017.06.001>
- [5] S.M. Hoseini, A. Heidarpour, S. Ghasemi, On the mechanism of mechanochemical synthesis of Ti<sub>2</sub>SC from Ti/FeS<sub>2</sub>/C mixture, *Adv. Powder Technol.* 30 (2019) 1672–1677, <https://doi.org/10.1016/j.apt.2019.05.017>
- [6] R.B. Mane, A. Haribabu, B.B. Panigrahi, Synthesis and sintering of Ti<sub>3</sub>GeC<sub>2</sub> MAX phase powders, *Ceram. Int.* 44 (2018) 890–893, <https://doi.org/10.1016/j.ceramint.2017.10.017>
- [7] D.T. Cuskelly, E.R. Richards, E.H. Kisi, V.J. Keast, Ti<sub>3</sub>GaC<sub>2</sub> and Ti<sub>3</sub>InC<sub>2</sub>: first bulk synthesis, DFT stability calculations and structural systematics, *J. Solid State Chem.* 230 (2015) 418–425, <https://doi.org/10.1016/j.jssc.2015.07.028>
- [8] X. Xu, Y. Bai, P. Jin, L. Li, X. Bai, G. Liu, C. Tang, First-principles calculations on the structural, elastic and electronic properties of a class of ternary carbides: a

- survey investigation, *Mater. Des.* 116 (2017) 331–339, <https://doi.org/10.1016/j.matdes.2016.12.032>
- [9] Q. Xu, Y. Zhou, H. Zhang, A. Jiang, Q. Tao, J. Lu, J. Rosén, Y. Niu, S. Grasso, C. Hu, Theoretical prediction, synthesis, and crystal structure determination of new MAX phase compound  $V_2SnC$ , *J. Adv. Ceram.* 9 (2020) 481–492, <https://doi.org/10.1007/s40145-020-0391-8>
- [10] E. Tabares, A. Jiménez-Morales, S.A. Tsipas, Study of the synthesis of MAX phase  $Ti_3SiC_2$  powders by pressureless sintering, *Bol. Soc. Esp. Cerám. Vidr.* 60 (2021) 41–52, <https://doi.org/10.1016/j.bsecv.2020.01.004>
- [11] Y. Zhao, S. Deng, H. Liu, J. Zhang, Z. Guo, H. Hou, First-principle investigation of pressure and temperature influence on structural, mechanical and thermodynamic properties of  $Ti_3AlC_2$  (A = Al and Si), *Comput. Mater. Sci.* 154 (2018) 365–370, <https://doi.org/10.1016/j.commatsci.2018.07.007>
- [12] L. Chen, G. Duan, X.F. Gao, C.L. Wang, Property of mono-vacancy in MAX phase  $M_3AC_2$  (M = Ti, A = Al, Si, or Ge): First-principles calculations, *Mod. Phys. Lett. B* 32 (2018) 1–7, <https://doi.org/10.1142/S0217984918501609>
- [13] M. Akhlaghi, S.A. Tayebifard, E. Salahi, M. Shahedi Asl, G. Schmidt, Self-propagating high-temperature synthesis of  $Ti_3AlC_2$  MAX phase from mechanically-activated Ti/Al/graphite powder mixture, *Ceram. Int.* 44 (2018) 9671–9678, <https://doi.org/10.1016/j.ceramint.2018.02.195>
- [14] R. Tomoshige, K. Ishida, H. Inokawa, Effect of added molybdenum on material properties of Zr2SC MAX phase produced by self-propagating high temperature synthesis, *Explosion Shock Waves and High Strain Rate Phenomena, MaterialsResearchForum LLC*, 2019, pp. 79–84, <https://doi.org/10.21741/9781644900338-14>
- [15] N. Abbas, X. Qin, S. Ali, G. Zhu, J. Lu, F.E. Alam, A.G. Wattoo, X. Zeng, K. Gu, J. Tang, Direct deposition of extremely low interface-contact-resistant  $Ti_2AlC$  MAX-phase coating on stainless-steel by mid-frequency magnetron sputtering method, *J. Eur. Ceram. Soc.* 40 (2020) 3338–3342, <https://doi.org/10.1016/j.jeurceramsoc.2020.02.033>
- [16] S.A. Hosseinizadeh, A. Pourebrahim, H. Baharvandi, N. Ehsani, Synthesis of nano-layered  $Ti_3SiC_2$  MAX phase through reactive melt infiltration (RMI): metallurgical and thermodynamical parameters, *Ceram. Int.* 46 (2020) 22208–22220, <https://doi.org/10.1016/j.ceramint.2020.05.298>
- [17] J. Lyu, E.B. Kashkarov, N. Travitzky, M.S. Syrtanov, A.M. Lider, Sintering of MAX-phase materials by spark plasma and other methods, *J. Mater. Sci.* 56 (2021) 1980–2015, <https://doi.org/10.1007/s10853-020-05359-y>
- [18] T. Yang, Q. Chen, X. Li, C. Meng, B. Ye, B. Gou, Low-temperature synthesis of  $Ti_3Al(Sn)C_2$  solid solution using replacement reaction, *J. Mater. Sci. Mater. Electron* 31 (2020) 20601–20610, <https://doi.org/10.1007/s10854-020-04580-4>
- [19] T. Rackl, L. Eisenburger, R. Niklaus, D. Johrendt, Syntheses and physical properties of the MAX phase boride  $Nb_2SB$  and the solid solutions  $Nb_2SB_xC_{1-x}$  ( $x = 0-1$ ), *Phys. Rev. Mater.* 3 (2019) 1–7, <https://doi.org/10.1103/PhysRevMaterials.3.054001>
- [20] T. Rackl, D. Johrendt, The MAX phase borides  $Zr_2SB$  and  $Hf_2SB$ , *Solid State Sci.* 106 (2020) 1–6, <https://doi.org/10.1016/j.solidstatesciences.2020.106316>
- [21] Y. Niu, S. Fu, K. Zhang, B. Dai, H. Zhang, S. Grasso, C. Hu, Synthesis, microstructure, and properties of high purity  $Mo_2TiAlC_2$  ceramics fabricated by spark plasma sintering, *J. Adv. Ceram.* 9 (2020) 759–768, <https://doi.org/10.1007/s40145-020-0412-7>
- [22] T.H. Scabarozzi, S. Amini, P. Finkel, O.D. Leaffer, J.E. Spanier, M.W. Barsoum, M. Drulis, H. Drulis, W.M. Tambussi, J.D. Hettinger, S.E. Lofland, Electrical, thermal, and elastic properties of the MAX-phase  $Ti_2SC$ , *J. Appl. Phys.* 104 (2008) 1–6, <https://doi.org/10.1063/1.2959738>
- [23] W.B. Zhu, J.H. Song, B.C. Mei, Kinetics and microstructure evolution of  $Ti_2SC$  during in situ synthesis process, *J. Alloy. Compd.* 566 (2013) 191–195, <https://doi.org/10.1016/j.jallcom.2013.03.032>
- [24] X. Li, B. Liang, Z. Li, Combustion synthesis of  $Ti_2SC$ , *104* (2013) 1038–1040.
- [25] W. Zhou, L. Liu, J. Zhu, S. Tian, Facile synthesis of high-purity  $Ti_2SC$  powders by spark plasma sintering technique, *Ceram. Int.* 43 (2017) 9363–9368, <https://doi.org/10.1016/j.ceramint.2017.04.104>
- [26] C. Guan, N. Sun, Synthesis and reaction evolution of high-purity  $Ti_2SC$  powder by microwave hybrid heating at low temperature, *Adv. Appl. Ceram.* 115 (2016) 499–504, <https://doi.org/10.1080/17436753.2016.1193992>
- [27] M. Opeka, J. Zaykoski, I. Talmy, S. Causey, Synthesis and characterization of  $Zr_2SC$  ceramics, *Mater. Sci. Eng. A* 528 (2011) 1994–2001, <https://doi.org/10.1016/j.msea.2010.10.084>
- [28] M. Romero, L. Huerta, T. Akachi, J.L.S. Llamazares, R. Escamilla, X-ray photoelectron spectroscopy studies of the electronic structure of superconducting  $Nb_2SnC$  and  $Nb_2SC$ , *J. Alloy. Compd.* 579 (2013) 516–520, <https://doi.org/10.1016/j.jallcom.2013.05.214>
- [29] M. Romeo, R. Escamilla, Pressure effect on the structural, elastic and electronic properties of  $Nb_2AC$  (A = S and In) phases; Ab initio study, *Comput. Mater. Sci.* 81 (2014) 184–190, <https://doi.org/10.1016/j.commatsci.2013.08.010>
- [30] S.R. Kulkarni, M. Merlini, N. Phatak, S.K. Saxena, G. Artioli, S. Amini, M.W. Barsoum, Thermal expansion and stability of  $Ti_2SC$  in air and inert atmospheres, *J. Alloy. Compd.* 469 (2009) 395–400, <https://doi.org/10.1016/j.jallcom.2008.01.150>
- [31] C.F. Hu, F.Z. Li, L.F. He, M.Y. Liu, J. Zhang, J.M. Wang, Y.W. Bao, J.Y. Wang, Y.C. Zhou, In situ reaction synthesis, electrical and thermal, and mechanical properties of  $Nb_4AlC_3$ , *J. Am. Ceram. Soc.* 91 (2008) 2258–2263, <https://doi.org/10.1111/j.1551-2916.2008.02424.x>
- [32] S. Fu, Y. Liu, H. Zhang, S. Grasso, C. Hu, Synthesis and characterization of high purity  $Mo_2Ti_2AlC_3$  ceramic, *J. Alloy. Compd.* 815 (2020) 152485, <https://doi.org/10.1016/j.jallcom.2019.152485>
- [33] A. Nastic, A. Merati, M. Bielawski, M. Bolduc, O. Fakolujo, M. Nganbe, Instrumented and Vickers indentation for the characterization of stiffness, hardness and toughness of zirconia toughened  $Al_2O_3$  and  $SiC$  armor, *J. Mater. Sci. Technol.* 31 (2015) 773–783, <https://doi.org/10.1016/j.jmst.2015.06.005>
- [34] A.A.H. Ameri, N.N. Elewa, M. Ashraf, J.P. Escobedo-Diaz, General methodology to estimate the dislocation density from microhardness measurements, *Mater. Charact.* 131 (2017) 324–330, <https://doi.org/10.1016/j.matchar.2017.06.031>
- [35] J. Gong, X. Pan, H. Miao, Z. Zhao, Effect of metallic binder content on the microhardness of  $TiCN$ -based cermets, *Mater. Sci. Eng. A* 359 (2003) 391–395, [https://doi.org/10.1016/S0921-5093\(03\)00396-4](https://doi.org/10.1016/S0921-5093(03)00396-4)
- [36] X. Su, J. Dong, L. Chu, H. Sun, S. Grasso, C. Hu, Synthesis, microstructure and properties of  $MoAlB$  ceramics prepared by in situ reactive spark plasma sintering, *Ceram. Int.* 46 (2020) 15214–15221, <https://doi.org/10.1016/j.ceramint.2020.03.059>